

## Nanosheets

Ruddlesden–Popper Hybrid Lead Bromide Perovskite Nanosheets of Phase Pure  $n = 2$ : Stabilized Colloids Stored in the Solid State

Rita B. Cevallos-Toledo, Ignacio Rosa-Pardo, Raul Arenal, Víctor Oestreicher, Michael Fickert, Gonzalo Abellán, Raquel E. Galian,\* and Julia Pérez-Prieto\*

**Abstract:** Ruddlesden–Popper lead halide perovskite (RP-LHP) nano-nanostructures can be regarded as self-assembled quantum wells or superlattices of 3D perovskites with an intrinsic quantum well thickness of a single or a few ( $n = 2-4$ ) lead halide layers; the quantum wells are separated by organic layers. They can be scaled down to a single quantum well dimension. Here, the preparation of highly (photo)chemical and colloidal stable hybrid LHP nanosheets (NSs) of ca.  $7.4\ \mu\text{m}$  lateral size and  $2.5\ \text{nm}$  quantum well height (thereby presenting a deep blue emission at ca.  $440\ \text{nm}$ ), is reported for the first time. The NSs are close-lying and they even interconnect when deposited on a substrate. Their synthesis is based on the use of the *p*-toluenesulfonic acid/dodecylamine (pTS/DDA) ligand pair and their (photo)chemical stability and photoluminescence is enhanced by adding  $\text{EuBr}_2$  nano-dots (EuNDs). Strikingly, they can be preserved as a solid and stored for at least one year. The blue emissive colloid can be recovered from the solid as needed by simply dispersing the powder in toluene and then using it to prepare solid films, making them very promising candidates for manufacturing devices.

Colloidal lead halide perovskites (LHPs) are relatively new semiconductor materials which are attracting great interest due to their outstanding optoelectronic properties.<sup>[1]</sup> The most studied materials present the  $\text{APbX}_3$  formula, where A is a small-sized organic or metal mono-cation and X is a halide anion and present a three-dimensional (3D) inorganic framework.<sup>[2]</sup> LHPs can also be prepared with other stoichiometries and different morphologies.<sup>[3]</sup> Among them, Ruddlesden–Popper (RP) lead halide perovskite nanostructures with  $\text{L}_2[\text{APbX}_3]_{n-1}\text{PbX}_4$  formula, where “L” usually represents a long-chain alkyl or aromatic ammonium ligand and “ $n$ ” is an

integer which stands for the number of lead halide layers held together by weak van der Waals interactions, and sandwiched between organic layers, are cutting-edge.<sup>[4]</sup> Maruyama et al. reported the first layered lead halide 2D-perovskite, specifically  $(\text{CH}_3(\text{CH}_2)_8\text{NH}_3)_2\text{PbI}_4$ ,<sup>[5]</sup> and soon after Ishihara et al.<sup>[6]</sup> analyzed the photophysical features of this type of materials.

Ruddlesden–Popper 2D nanostructures exhibit different features from those of typical 2D perovskites: i) they are integrated by quantum well structures, thereby exhibiting a strong quantum confinement due to their thickness (below the Bohr radius of the material); ii) the quantum confinement occurs without physically thinning the material down to the atomic thickness; and consequently iii) the emission peaks appear at the same wavelength as long as the  $[\text{A}_{n-1}\text{Pb}_n\text{X}_{3n+1}]$  layer thickness is homogeneous, independently of its lateral dimensions; iv) the excitonic absorption and emission peaks are exceptionally narrow, with a small Stokes shift ( $< 10\ \text{meV}$ ).

Moreover, the successful manufacture of atomically thin nanosheets with  $n = 1$  reported by Yang et al. in 2015<sup>[7]</sup> has shown that the preparation of individually dispersed materials with a single quantum well is feasible.

Perovskite nanosheets with a strong quantum confinement (quantum wells with 1–4 lead halide layers) exhibit a blue-shifted emission compared to the bulk phase.<sup>[8]</sup>

Among many exciting characteristics of these perovskite nanostructures, the excellent optoelectronic properties, such as their large absorption coefficient, high carrier mobility and long diffusion length, make them promising materials for energy-related devices, including photodetectors, light-emitting diodes (LEDs), and solar cells.<sup>[9]</sup> Namely, LHP nanostructures with a large lateral size, such as NSs, would be easy to incorporate into optical or electronic devices; furthermore,

[\*] R. B. Cevallos-Toledo, I. Rosa-Pardo, Dr. V. Oestreicher, Dr. G. Abellán, Dr. R. E. Galian, Prof. J. Pérez-Prieto  
Institute of Molecular Science, University of Valencia  
c/ Catedrático José Beltrán 2, Paterna (Spain)  
E-mail: raquel.galian@uv.es  
Julia.perez@uv.es  
Dr. R. Arenal  
Laboratorio de Microscopías Avanzadas (LMA), U. Zaragoza  
Mariano Esquillor s/n, 50018 Zaragoza (Spain)  
and  
Instituto de Nanociencia y Materiales de Aragón (INMA), CSIC-U. de Zaragoza  
Calle Pedro Cerbuna 12, 50009 Zaragoza (Spain)  
and  
ARAID Foundation  
50018 Zaragoza (Spain)

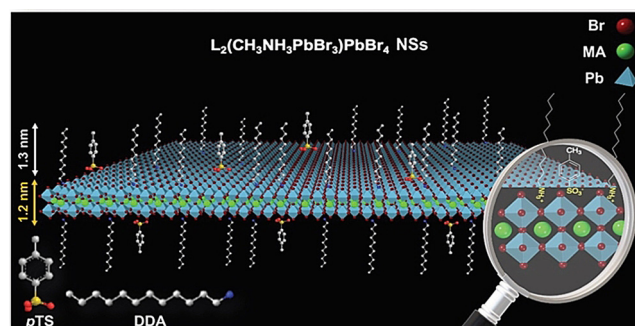
M. Fickert  
Department of Chemistry and Pharmacy, Chair of Organic Chemistry II and Joint Institute of Advanced Materials and Processes (ZMP), Friedrich-Alexander-Universität Erlangen-Nürnberg (FAU), Nikolaus-Fiebiger Strasse 10, 90762 Erlangen (Germany) and Friedrich-Alexander-Universität Erlangen-Nürnberg (FAU) Dr.-Mack Strasse 81, 90762 Fürth (Germany)

Supporting information and the ORCID identification number(s) for the author(s) of this article can be found under: <https://doi.org/10.1002/anie.202113451>.

© 2021 The Authors. Angewandte Chemie International Edition published by Wiley-VCH GmbH. This is an open access article under the terms of the Creative Commons Attribution License, which permits use, distribution and reproduction in any medium, provided the original work is properly cited.

they could be used to improve the moisture tolerance of 3D materials.<sup>[10,11]</sup> However, they present poor chemical stability, especially those of a single quantum well dimension, as they tend to evolve to a mixture of quantum wells with different thicknesses, and consequently to a material with a considerably broad emission.<sup>[9a,b,12]</sup> The preparation of films by assembling quantum wells differing in their thickness has been envisaged as an opportunity to perform nonradiative energy transfer between them and consequently to prepare tailor-made energy cascade nanostructures of interest in optoelectronics, but the assembly stability needs to be improved.<sup>[13]</sup>

The surface chemistry of LHPs has been extensively studied.<sup>[14]</sup> The ionic character of perovskites favors electrostatic interactions between the anchoring group and the perovskite surface. A dynamic equilibrium of bound-unbound ligands plays a key role in their colloidal stability and emissive properties. The sulfonate anion is a good coordinating ligand of the Pb ions at the perovskite surface; in particular, the use of *p*-didodecylbenzenesulfonate (*p*DBS) as the only coordinating ligand leads to 3D, green-emissive nanomaterial.<sup>[15]</sup> Considering the high acidity of sulfonic acids ( $pK_a = -5.4$  for *p*-toluenesulfonic acid, *p*TS),<sup>[16]</sup> which should protonate amines, we embarked on the preparation of strongly quantum-confined colloidal nanosheets (NSs) of 3D perovskites with a thickness of two lead halide layers by using *p*TS and a long alkyl (dodecylamine, DDA) ligand pair (Scheme 1), named LHP@DDA/*p*TS NSs. There are similarities between these NSs, phase  $n=1$  2D perovskite structures<sup>[7]</sup> and those with phase control of RP perovskites prepared in aqueous media.<sup>[17]</sup>



**Scheme 1.** Representative image of LHP@DDA/*p*TS NSs, with a thickness of two lead halide layers, capped with the *p*TS/DDA ligand pair.

The enhanced stabilization of the NSs by adding colloidal  $\text{EuBr}_2$  nanodots ( $\text{EuNDs}$  of ca. 2.2 nm in diameter) is reported here.

The preparation of LHP@DDA/*p*TS NSs was attempted by means of the ligand-assisted reprecipitation technique,<sup>[18]</sup> using a 1:1 methyl ammonium bromide (MABr)/ $\text{PbBr}_2$  molar ratio and DDA and *p*TS as the organic ligands, which were added using two different strategies: i) precursor solution was added to a DDA/*p*TS mixture, and then injected into toluene and ii) precursor solution was added to DDA (solid), and the resulting solution injected into a *p*TS toluene solution (Figure 1a). Both colloids showed basically two excitonic peaks (at 430 nm and 510 nm) and two emission peaks (at 434 nm and 534 nm); these optical features were consistent with the formation of NSs with a thickness of two lead halide layers and 3D ( $\text{MAPbBr}_3$ ) perovskite nanoparticles, respectively.

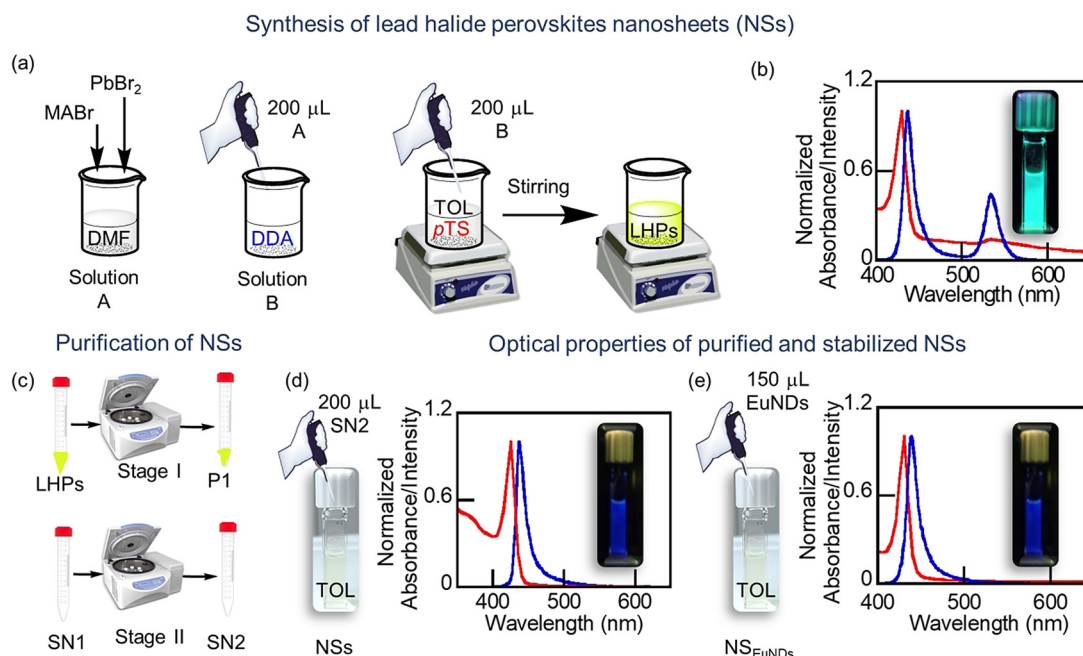


**Figure 1.** a) Scheme of the LHP@DDA/*p*TS NSs synthesis prepared by adding a precursor solution A into a DDA (solid) to form a solution B, which it was injected into a toluene solution containing *p*TS; b) normalized absorption and emission spectra ( $\lambda_{\text{ex}} = 365$  nm) of LHPs recorded after the synthesis without any purification step; c) Scheme of the purification of NSs; d), e) normalized absorption and emission spectra ( $\lambda_{\text{ex}} = 365$  nm) of the LHP@DDA/*p*TS NSs and LHP@DDA/*p*TS- $\text{EuNDs}$  NSs; inset: photograph of the colloidal dispersion (d) and of the film (e) under UV light.

However, the second strategy led to a better colloid in terms of dispersibility and purity (formation of only two emissive species), and predominance of the NSs (see Figures S1 and 1b). Different MABr/PbBr<sub>2</sub> and DDA/*p*TS molar ratios were evaluated, and the data are summarized in Table S1. Briefly, the optimal conditions to eventually obtain the NSs were by using MABr/PbBr<sub>2</sub>, *p*TS/DDA, and MA/DDA molar ratios of 0.8:1.0, 0.7:1.0 and 0.55:1, respectively, and toluene as the solvent (see SI experimental section for more details). Two centrifugation steps (stages I and II in Figure 1c) were carried out for the purification of the NSs, after which the second supernatant was selected (SN2). It exhibited the expected optical features for the pure NSs (exciton peak at 434 nm, full width half maximum, FWHM = 17 nm, and blue emission at 439 nm, FWHM = 14 nm; see Figure 1d). This material was termed LHP@DDA/*p*TS NSs (Scheme 1) and was further characterized by a battery of techniques (see below). Comparatively, the use of DDA as the only organic ligand produced perovskites with a 2D framework (emission peak at 405 nm),<sup>[3b]</sup> while *p*TS led to the 3D framework material (peak at 536 nm) just as *p*DBS<sup>[15]</sup> would, see Figure S2.

Although we succeeded in preparing pure, blue emissive NSs, they slowly evolved to other stoichiometries, as shown by the appearance of additional emission peaks at 456 nm and 520 nm, ascribed to NSs with a thickness of three lead halide layers and 3D (MAPbBr<sub>3</sub>) nanoparticles, respectively (see Figure S3a). Therefore, to enhance the chemical stability of the NSs, we used a previously reported strategy but with some modifications.<sup>[19,20]</sup> Specifically, an aliquot of a dispersion of EuNDs (0.02 mg mL<sup>-1</sup>) was added to the as-synthesized colloidal LHP NSs and the material was separated by centrifugation (see experimental section in SI for further

details). The LHP@DDA/*p*TS<sub>EuND</sub> NSs retained the optical properties of the LHP@DDA/*p*TS NSs (exciton and emission peaks at 431 nm and 439 nm, respectively, Figure 1e and Figure S4), and increased their chemical stability over time (Figure S3b) as well as under the electron beam of the transmission electron microscope (TEM, compare Figure 2a and Figure S5). Moreover, the photostability of the colloids under irradiation at 365 nm in air at 700 V using a Xe lamp demonstrated the higher photostability of LHP@DDA/*p*TS<sub>EuND</sub> (Figure S6). Time-resolved measurements showed the photoluminescence (PL) lifetimes of LHP@DDA/*p*TS<sub>EuND</sub> fitted to three components, resulting in PL average lifetimes ( $\tau_{av}$ ) of  $37.7 \pm 0.8$  ns for LHP@DDA/*p*TS<sub>EuND</sub> and  $39 \pm 1$  ns for LHP@DDA/*p*TS, thereby indicating the negligible effect of the EuNDs on the PL lifetime of the NSs. However, the PL quantum yield ( $\Phi_{PL}$ ) of the LHP@DDA/*p*TS<sub>EuND</sub> NSs nearly doubled that of the LHP@DDA/*p*TS NSs ( $\Phi_{PL} = 20\%$  and  $11\%$ , respectively). The size and morphology of the LHP@DDA/*p*TS<sub>EuND</sub> NSs were analyzed by TEM and atomic force microscopy (AFM); see Figure 2. TEM images showed the formation of squared NSs of about 7.4  $\mu\text{m}$  in lateral size (Figure 2a). High-angle annular dark-field scanning TEM (HAADF-STEM) images (Figure 2b) and energy dispersive X-ray spectroscopy (EDS-STEM) analyses shown in Figure 2c demonstrated that some EuNDs could be observed at the edge of the NSs. Figures 2d and S7 show characteristic topographic images obtained by AFM of different LHP@DDA/*p*TS<sub>EuND</sub> NSs isolated on a SiO<sub>2</sub>/Si substrate. Typically, the width of the NSs was on the  $\mu\text{m}$  scale, showing a strong aggregation of different nanosheets. The line profiles displayed terraces with well-marked steps showing the different step sizes that were present in the sample with

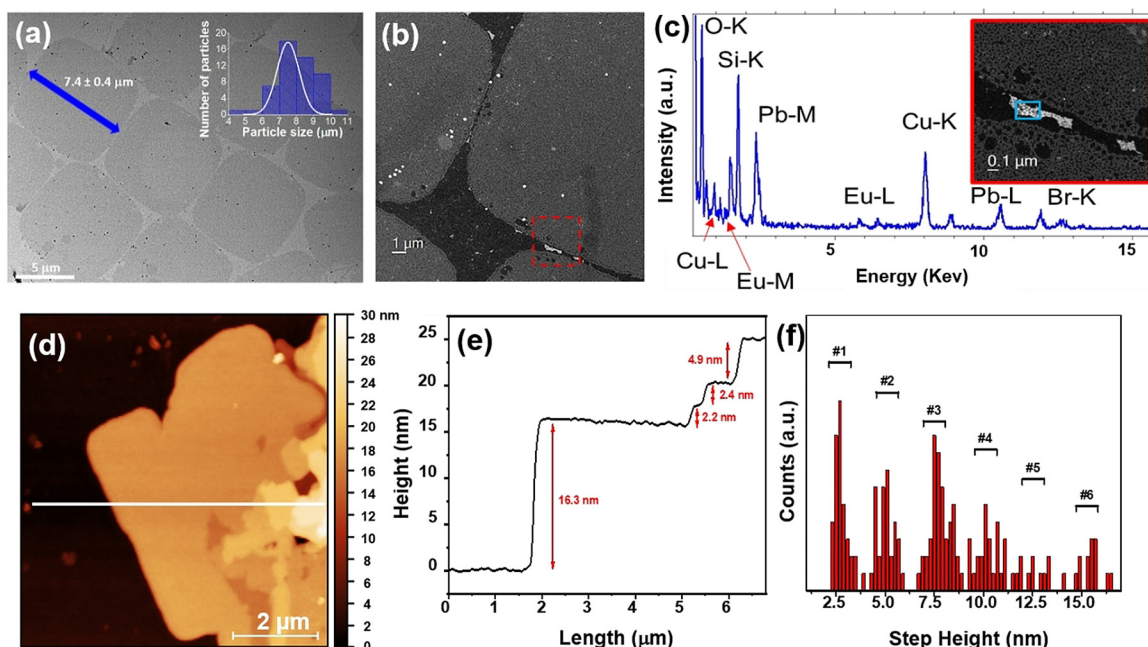


**Figure 2.** a) TEM image (scale bar 5  $\mu\text{m}$ ) and the corresponding histogram. b) HAADF-STEM image of some NSs; an enlargement can be seen in the red square highlighted in the micrograph, see the inset of the spectrum in (c). c) EDS spectrum collected in the area marked in blue, showing the presence of Eu as well as the other NPL elements. d), e) AFM images of LHP@DDA/*p*TS<sub>EuND</sub>s on a SiO<sub>2</sub>/Si substrate and the corresponding line profiles showing the height of the flakes; f) the statistical distribution of the different step heights can be observed in the LHP NSs.



a minimum thickness of ca. 2.2–2.5 nm (Figure 2 e). These data are consistent with  $\text{L}_2[\text{CH}_3\text{NH}_3\text{PbBr}_3]\text{PbBr}_4$  NSs formed by two metal lead halide layers (lead halide octahedral size of ca. 0.6 nm)<sup>[21]</sup> and a ligand layer formed by DDA and *p*TS (ca. 1.3 nm). AFM measurements were performed to analyze the distribution of the different heights; statistics and counts of the step heights accumulated at ca. 2.5 nm, 5 nm, 7.5 nm, 10 nm are shown in the histogram (all heights being multiples of about 2.5 nm); see Figure 2 f.

Astonishingly, drying the colloidal  $\text{LHP@DDA/pTS}_{\text{EuND}}$  yielded a yellow powder which remained stable for at least one year; it did not require any special conditions (specifically, it did not need to be stored in darkness or in an inert atmosphere). Moreover, blue-emissive NSs were recovered as needed by simply dispersing the powder in toluene without adding extra amounts of ligands (Figure 3); therefore, the

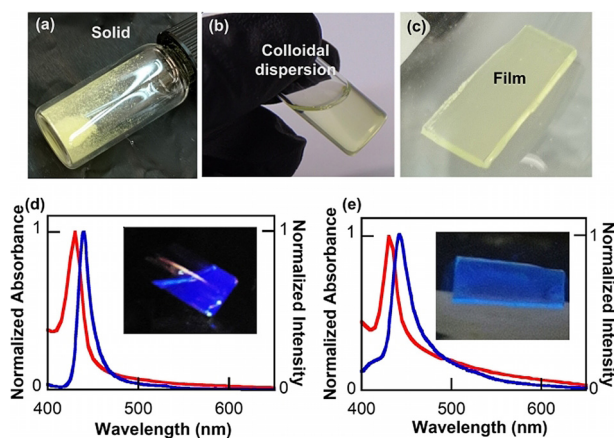


**Figure 3.** The  $\text{LHP@DDA/pTS}_{\text{EuND}}$  solid (a) can be redispersed in toluene to get a colloidal dispersion of the NSs (b), which can be used to prepare a film in a quartz substrate (c) under centrifugal casting. d), e) Normalized absorption and emission spectra of the colloidal dispersion and film of the  $\text{LHP@DDA/pTS}_{\text{EuND}}$  NSs.

solid acts as an excellent NS source. A blue-emissive solid-state NS film was prepared by depositing the  $\text{LHP@DDA/pTS}_{\text{EuND}}$  NS colloid onto a quartz substrate (hydrophobic side) and, surprisingly, it preserved its main optical properties (excitonic and emission peaks at 431 nm and 442 nm, respectively, see Figure 3 and SI for further details).

The powder X-ray diffraction (XRD) spectra of the  $\text{LHP@DDA/pTS}$  colloid before purification (whose absorption and emission spectra are shown in Figure 1 b) and that of RP-LHP of phase pure  $n=2$  stabilized with EuNDs ( $\text{LHP@DDA/pTS}_{\text{EuND}}$ ) were analyzed in a capillary tube (see further details in the SI). The former showed a set of sharp and intense peaks at low 2-theta values (see Figure S8a), with reflection expected for the NSs stacked at regular intervals<sup>[22]</sup> associated with an average spacing between layered NSs of ca. 27 Å, denoted as 00 $l$ . Interestingly, this value matched well with the AFM measurements (Figure 2 d–f), suggesting that this is the minimal structural unit constituting the hybrid material and were consistent with the chemical composition of the NSs (Scheme 1). Another set

of signals attributable to an average spacing between layered NSs of ca. 32 Å, denoted as 00 $l$ , were also observed but with very low intensities. These two sets of reflections can be associated with different orientations and/or packing of the organic layers. Similar strong reflections have also been observed in hybrid perovskite nanoplatelets with large lateral sizes prepared in thin films, along with the typical peaks from atomic plane reflections 100 and 200.<sup>[21]</sup> The additional peaks can be attributed to diffraction planes of the organic ligands and perovskite precursor salts (see Figure S8c for  $\text{PbBr}_2$ ).<sup>[24]</sup> In fact, these peaks did not appear in the purified  $\text{LHP@DDA/pTS}$  sample, whose absorption and emission spectra are shown in Figure 1 e and correspond to RP-LHP phase pure  $n=2$ . The lack of an exact X-ray structure for this material impeded the perfect assignment of the peaks. However, the lamellar nature was satisfactorily confirmed.

With respect to  $\text{LHP@DDA/pTS}_{\text{EuND}}$ , the mixing of the colloidal thin nanosheets with EuNDs followed by drying hindered the stacking and facilitated the observation of the perovskite atomic plane reflections (Figure S8b). Similar observations have been reported by Tisdale et al., who added silica particles to colloidal nanoplatelets before their deposition to form a film.<sup>[21]</sup>

The XRD pattern of both samples showed the typical diffraction peaks, located at 15.03° (100), 21.40° (110), 30.30° (200) and 33.90° (210), which are characteristic of crystalline 3D perovskites, with higher intensity for the 100 diffraction plane<sup>[21]</sup> (Figure S8a,b). Moreover, the two sharp and intense signals centered at ca. 15° and 30° correspond to the distance between two Pb octahedral centers (5.9 Å).<sup>[21]</sup>

The solid was further characterized by X-Ray photoelectron spectroscopy (XPS), attenuated total reflectance Fourier-Transform infrared spectroscopy (ATR-FTIR), thermogravimetric analysis coupled with gas chromatography and mass spectrometry (TG-GC-MS), and  $^1\text{H-NMR}$  (*d*-DMSO); this information is compiled in the ESI (Figure S9–S24 and Tables S2–S6).

Therefore, the DDA/*p*TS ligand pair brought about the confinement of the perovskite material in two dimension to produce  $\mu\text{m}$ -sized quantum confined nanosheets of 3D perovskites with a thickness of two lead halide layers, while the EuNDs gave them chemical stability. In organic solvents, the perovskite NSs tend to partially evolve into NSs with thicker quantum wells. This can be attributed to a dynamic equilibrium of bound-unbound ligands on the NS surface in the organic solvent. The EuNDs seem to help in the stabilization of colloidal NSs by establishing a weak interaction between the EuNDs ligands (with a radial distribution on the nanodot surface) and those of the NSs (with a parallel distribution on the NS surface). Thereby, the EuNDs prevented the NSs from a structural rearrangement and/or coalescence and made the recovery of the colloidal NSs from the solid possible (similar optical properties as the as-synthesized NSs, see Figures 1 d,e).

To see the specificity of EuNDs in the stabilization of the NSs, semiconductor nanoparticles of CdSe with similar size (2.2 nm) and the same organic ligands to that of the EuNDs (DDA/myristic acid, see experimental section for further details and Figure S25) were also tested. In both cases,

addition of the colloid stabilized the nanosheets for at least 8 h (Figure S3c), but the perovskite material was steadily destroyed under prolonged periods in the presence of CdSe. This can be attributed to a weak ligand-CdSe interaction, thus eventually resulting in perovskite damage.

As mentioned above, the difficulties involved in preparing films from blue-emitting hybrid perovskite NSs are well known. Their preparation by using anti-solvent or hot injection procedures results in a low NS concentration, while evaporation and centrifugation procedures, used to increase the concentration, destroy the NS surface, and give rise to agglomeration or staked superstructures.

Remarkably, the long-term stability in the solid state together with the high processability of the NS colloid herein synthesized enabled the preparation of blue-emissive solid films, which may be suitable for assembling on a large area on demand and, consequently, be useful for preparing high-quality films for flexible and ultrathin optoelectronic devices, or they could be combined with other types of 2D materials, through a simple solution process, such as, an ink-printing method. Research work for this falls outside the scope of this paper but we expect to address it in the near future.

## Acknowledgements

The work was supported by the Spanish MICINN (CTQ2017-82711-P, PID2020-115710GB-I00/AEI/10.13039/501100011033, FPU17/05564 (IRP), partially co-financed with FEDER funds, PID2019-111742GA-I00, PID2019-104739GB-I00/AEI/10.13039/501100011033, and the “Maria de Maeztu” Programme for Units of Excellence in R&D (CEX2019-000919-M)) and the European Union (ERC-2018-StG 804110-2D-PnitoChem to G.A., “ESTEEM3” (823717) and Graphene Flagship (881603) to R.A.). The authors also thank the financial support by Generalitat Valenciana (PROMETEO/2019/080 and IDIFEDER/2018/064 to J.P.P., Santiago Grisolia (RCT), CIDEAGENT/2018/001 and IDIFEDER/2018/061 co-financed by FEDER to G.A.), the Government of Aragon (project DGA E13-20R) and the Deutsche Forschungsgemeinschaft (DFG, FLAG-ERA AB694/2-1 to G.A.). EDS-STEM analyses have been performed at the Laboratorio de Microscopias Avanzadas, Universidad de Zaragoza, Spain. V.O. is an ALN fellow.

## Conflict of Interest

The authors declare no conflict of interest.

**Keywords:** colloids · film · lead halide perovskites · nanodots · nanosheets

- [1] a) A. K. Jena, A. Kulkarni, T. Miyasaka, *Chem. Rev.* **2019**, *119*, 3036–3103; b) V. Blay, R. E. Galian, L. M. Muresan, D. Pankratov, P. Pinyou, G. Zampardi, *Adv. Sustainable Syst.* **2020**, *4*, 1900145; c) A. Dey, J. Ye, A. De, E. Debroye, S. K. Ha, E. Bladt, A. S. Kshirsagar, Z. Wang, J. Yin, Y. Wang, L. N. Quan, F. Yan, M. Gao, X. Li, J. Shamsi, T. Debnath, M. Cao, M. A. Scheel, S. Kumar, J. A. Steele, M. Gerhard, L. Chouhan, K. Xu, X.-g. Wu, Y. Li, Y. Zhang, A. Dutta, C. Han, I. Vincon, A. L. Rogach, A. Nag, A. Samanta, B. A. Korgel, C.-J. Shih, D. R. Gamelin, D. H. Son, H. Zeng, H. Zhong, H. Sun, H. V. Demir, I. G. Scheblykin, I. Mora-Seró, J. K. Stolarczyk, J. Z. Zhang, J. Feldmann, J. Hofkens, J. M. Luther, J. Pérez-Prieto, L. Li, L. Manna, M. I. Bodnarchuk, M. V. Kovalenko, M. B. J. Roeflaers, N. Pradhan, O. F. Mohammed, O. M. Bakr, P. Yang, P. Müller-Buschbaum, P. V. Kamat, Q. Bao, Q. Zhang, R. Krahne, R. E. Galian, S. D. Stranks, S. Bals, V. Biju, W. A. Tisdale, Y. Yan, R. L. Z. Hoyer, L. Polavarapu, *ACS Nano* **2021**, *15*, 10775–10981.
- [2] D. B. Mitzi in *Progress in Inorganic Chemistry*, Vol. 58 (Ed.: K. D. Karlin), Wiley, New York, **2014**, p. 528.
- [3] a) S. Gonzalez-Carrero, R. E. Galian, J. Pérez-Prieto, *Opt. Express* **2016**, *24*, A285–A301; b) S. Gonzalez-Carrero, G. M. Espallargas, R. E. Galian, J. Pérez-Prieto, *J. Mater. Chem. A* **2015**, *3*, 14039–14045; c) S. Gonzalez-Carrero, L. C. Schmidt, I. Rosa-Pardo, L. Martínez-Sarti, M. Sessolo, R. E. Galian, J. Pérez-Prieto, *ACS Omega* **2018**, *3*, 1298–1303.
- [4] L. Mao, C. C. Stoumpos, M. G. Kanatzidis, *J. Am. Chem. Soc.* **2019**, *141*, 1171–1190.
- [5] Y. I. Dolzhenko, T. Inabe, Y. Maruyama, *Bull. Chem. Soc. Jpn.* **1986**, *59*, 563–567.
- [6] T. Ishihara, J. Takahashi, T. Goto, *Solid State Commun.* **1989**, *69*, 933–936.
- [7] L. Dou, A. B. Wong, Y. Yu, M. Lai, N. Kornienko, S. W. Eaton, A. Fu, C. G. Bischak, J. Ma, T. Ding, N. S. Ginsberg, L.-W. Wang, A. P. Alivisatos, P. Yang, *Science* **2015**, *349*, 1518.
- [8] K. Leng, I. Abdelwahab, I. Verzhbitskiy, M. Telychko, L. Chu, W. Fu, X. Chi, N. Guo, Z. Chen, Z. Chen, C. Zhang, Q.-H. Xu, J. Lu, M. Chhowalla, G. Eda, K. P. Loh, *Nat. Mater.* **2018**, *17*, 908–914.
- [9] a) S. Kumar, J. Jagielski, S. Yakunin, P. Rice, Y.-C. Chiu, M. Wang, G. Nedelcu, Y. Kim, S. Lin, E. J. G. Santos, M. V. Kovalenko, C.-J. Shih, *ACS Nano* **2016**, *10*, 9720–9729; b) H. Fang, W. Deng, X. Zhang, X. Xu, M. Zhang, J. Jie, X. Zhang, *Nano Res.* **2019**, *12*, 171–176; c) C. Lan, Z. Zhou, R. Wei, J. C. Ho, *Mater. Today Energy* **2019**, *11*, 61–82.
- [10] Note: Hybrid 3D/2D perovskites have shown higher ambient stability than pure 3D perovskites. (see reference [8]).
- [11] a) T. M. Koh, V. Shanmugam, X. Guo, S. S. Lim, O. Filonik, E. M. Herzig, P. Müller-Buschbaum, V. Swamy, S. T. Chien, S. G. Mhaisalkar, N. Mathews, *J. Mater. Chem. A* **2018**, *6*, 2122–2128; b) M. C. Gélvez-Rueda, M. B. Fridriksson, R. K. Dubey, W. F. Jager, W. van der Stam, F. C. Grozema, *Nat. Commun.* **2020**, *11*, 1901.
- [12] a) J. A. Sichert, Y. Tong, N. Mutz, M. Vollmer, S. Fischer, K. Z. Milowska, R. García Cortadella, B. Nickel, C. Cardenas-Daw, J. K. Stolarczyk, A. S. Urban, J. Feldmann, *Nano Lett.* **2015**, *15*, 6521–6527; b) Y. Bekenstein, B. A. Koscher, S. W. Eaton, P. Yang, A. P. Alivisatos, *J. Am. Chem. Soc.* **2015**, *137*, 16008–16011; c) J. Shamsi, Z. Dang, P. Bianchini, C. Canale, F. Di Stasio, R. Brescia, M. Prato, L. Manna, *J. Am. Chem. Soc.* **2016**, *138*, 7240–7243.
- [13] a) A. Singldinger, M. Gramlich, C. Gruber, C. Lampe, A. S. Urban, *ACS Energy Lett.* **2020**, *5*, 1380–1385; b) M. Yuan, L. N. Quan, R. Comin, G. Walters, R. Sabatini, O. Voznyy, S. Hoogland, Y. Zhao, E. M. Beauregard, P. Kanjanaboos, Z. Lu, D. H. Kim, E. H. Sargent, *Nat. Nanotechnol.* **2016**, *11*, 872–877.
- [14] a) R. E. Galian, J. Pérez-Prieto in *Research Perspectives on Functional Micro- and Nanoscale Coatings* (Eds.: A. Zuzuarregui, M. C. Morant-Miñana), IGI Global, Hershey, **2016**, pp. 42–77; b) A. Zuzuarregui, M. C. Morant-Miñana in *Research Perspectives on Functional Micro- and Nanoscale Coatings* (Eds.: A. Zuzuarregui, M. C. Morant-Miñana), IGI Global, Hershey, **2016**, pp. 1–25.

- [15] D. Yang, X. Li, W. Zhou, S. Zhang, C. Meng, Y. Wu, Y. Wang, H. Zeng, *Adv. Mater.* **2019**, *31*, 1900767.
- [16] J. P. Guthrie, *Can. J. Chem.* **2017**, *01*, 2342–2354.
- [17] D. Pan, Y. Fu, N. Spitha, Y. Zhao, C. R. Roy, D. J. Morrow, D. D. Kohler, J. C. Wright, S. Jin, *Nat. Nanotechnol.* **2021**, *16*, 159–165.
- [18] F. Zhang, H. Zhong, C. Chen, X.-g. Wu, X. Hu, H. Huang, J. Han, B. Zou, Y. Dong, *ACS Nano* **2015**, *9*, 4533–4542.
- [19] Note: We have previously reported on the preparation of two-layered [CsPbBr<sub>3</sub>]/PbBr<sub>4</sub> platelets, which were relatively chemically stable with low dispersibility in toluene, by using ultrasound/heating post-treatment of toluene dispersions of CsPbBr<sub>3</sub> micro-sized wires in the presence of EuBr<sub>2</sub> nanodots (EuNDs).
- [20] I. Rosa-Pardo, S. Pocoví-Martínez, R. Arenal, R. E. Galian, J. Pérez-Prieto, *Nanoscale* **2019**, *11*, 18065–18070.
- [21] M. C. Weidman, M. Seitz, S. D. Stranks, W. A. Tisdale, *ACS Nano* **2016**, *10*, 7830–7839.
- [22] C. C. Stoumpos, D. H. Cao, D. J. Clark, J. Young, J. M. Rondinelli, J. I. Jang, J. T. Hupp, M. G. Kanatzidis, *Chem. Mater.* **2016**, *28*, 2852–2867.
- [23] a) L. C. Schmidt, A. Pertegás, S. González-Carrero, O. Malinkiewicz, S. Agouram, G. Mínguez Espallargas, H. J. Bolink, R. E. Galian, J. Pérez-Prieto, *J. Am. Chem. Soc.* **2014**, *136*, 850–853; b) A. Jancik Prochazkova, M. C. Scharber, C. Yumusak, J. Jančík, J. Másilko, O. Brüggemann, M. Weiter, N. S. Sariciftci, J. Krajcovic, Y. Salinas, A. Kovalenko, *Sci. Rep.* **2020**, *10*, 15720.
- [24] N. Kawano, M. Koshimizu, G. Okada, Y. Fujimoto, N. Kawaguchi, T. Yanagida, K. Asai, *Sci. Rep.* **2017**, *7*, 14754.

Manuscript received: October 4, 2021

Accepted manuscript online: October 21, 2021

Version of record online: November 10, 2021